Bearings-Only Guidance in Cis-Lunar Rendezvous*

Fabio D'Onofrio † and Giordana Bucchioni‡
University of Pisa, 56122 Pisa, Italy

Mario Innocenti§
University of Pisa, Pisa, 56122 Pisa, Italy

*

I. Introduction

In recent years international space agencies, and commercial companies have started programming a permanent return to the Moon and future manned missions to Mars. A general consensus for the return to the Moon is the use of a permanent space station in lunar orbit, currently denoted as Lunar Orbital Platform-Gateway (LOP-G), which will serve as a short-term habitation module, science laboratory, and transfer area for rovers and Moon landers.

The Human-Enhanced Robotic Architecture and Capability for Lunar Exploration and Science program HERACLES [1], provided a multi-agency baseline study for a lander, whose aim is to collect Moon samples and return them to the Earth using NASA Orion spacecraft, leveraging the LOP-G as a staging point.

This space infrastructure will follow a particular type of orbit that has been widely studied in orbital mechanics since the 1960s, but has never been used by now for a real manned space mission: a Near Rectilinear Halo Orbit (NRHO). Such orbits offer long-term stability, with low propellant requirements for orbital station-keeping, by exploiting a balance point in the gravitational field of Earth and Moon [2]. Indeed, the gravitational interaction between our planet and its natural satellite makes possible several highly non-Keplerian orbits, among which the NRHO was selected because of its high eccentricity and orientation, which ensure continuous contact with Earth.

Rendezvous and proximity operations with the Gateway will require the development of suitable guidance, navigation, and control (GNC) algorithms, which must take into account the complex dynamic environment. In this work, in particular, the chaser vehicle is assumed to be able to measure relative angles to the target only, which is passive in its NRHO. One of the main reasons for using angular measurements only for rendezvous is the advantage in terms of required power, weight and costs that optical navigation systems can provide [3]. In addition, radio-type relative navigation could not be feasible if the target is uncooperative.

The Autonomous Vision Approach Navigation and Target Identification (AVANTI) experiment successfully

*A limited version of the paper was presented at the 31st AAS/AIAA Space Flight Mechanics Meeting, as AAS-21-209.
†Graduate student, Department of Information Engineering, Via Caruso 16, f.donofrio6@studenti.unipi.it.
‡Ph.D. Candidate, Department of Information Engineering, Via Caruso 16, giordana.bucchioni@ing.unipi.it.
§Professor, Department of Information Engineering, Via Caruso 16, mario.innocenti@unipi.it, Associate Fellow AIAA.
*Presented at the 31st AAS/AIAA Space Flight Mechanics Meeting, Paper 21-209, Charlotte, NC, USA, February 1-3, 2021

demonstrated angles-only navigation for rendezvous between two smallsats in low Earth Orbit (LEO) [4]. The chaser vehicle was able to extract the line-of-sight observations from the images taken by a monocular camera, through a dedicated target detection algorithm.

The ability to perform fully autonomous navigation through vision-based sensors is also a key-enabling technology for future mission concepts involving spacecraft swarms in deep-space [5].

The major downside of bearings-only navigation is the difficulty in determining the range. Woffinden and Geller [6] and Grzymisch and Fichter [7] provided closed-form sufficient conditions for observability in the framework of the Hill-Clohessy-Wiltshire (HCW) equations valid for target circular orbits [8]. Luo et al. [9] extended the analysis to the Tschauner - Hempel (TH) model, which provides the equations valid for eccentric orbits [10]. The common conclusion about using angles-only relative navigation in conjunction with linear models for relative motion, such as the HCW and TH equations, is that maneuvers must be performed by the chaser in order to reconstruct the relative range from bearings measurements. This is the approach taken, for instance, by Woffinden and Geller [11] and Grzymisch and Fichter [12].

In all the aforementioned literature, the gravitational pull of a single primary is considered in spacecraft dynamic modelling, therefore neglecting third-body effects. When the target follows a highly non-Keplerian orbit such as a NRHO about a collinear Lagrange point in the Earth-Moon system, relative motion models based on the two-body problem perform poorly. To this date, there are no applications of angles-only relative navigation to rendezvous and proximity operations in such scenarios characterized by a dynamic environment substantially different from low Earth orbit.

This Note proposes the application of a fuel-observability optimal rendezvous guidance with angles-only navigation, as introduced by Grzymisch and Fichter [13], to a three-body problem scenario relevant for the next Moon missions. Indeed, in that work, the authors assumed a circular target orbit, therefore the relative motion equations exploited by the guidance algorithm were the HCW. Here the equations of relative motion between the two spacecraft are based on either the Elliptic Restricted Three-Body Problem (ER3BP) or the Circular Restricted Three-Body Problem (CR3BP), and are expressed in a target-centered Local-Vertical Local-Horizontal (LVLH) frame [14], well suited for guidance and control applications.

The observability cost is defined on the basis of third-body perturbed linearized relative dynamics, and it is then used in an online guidance algorithm to optimize a trade-off between observability and fuel consumption. The relative translational state is periodically updated by the navigation system, which consists of an angles-only Extended Kalman Filter (EKF) exploiting the nonlinear three-body dynamics and spherical coordinates for the measurement equations.

The remainder of the paper is structured as follows: Sec. II reviews the relative motion models based on a three-body dynamics; Sec. III describes the rendezvous scenario; Sec. IV summarizes the bearings-only guidance and navigation algorithms. Simulation results are reported in Sec. V, and conclusions are drawn in Sec. VI.

II. Relative Motion in the Restricted Three-Body Problem

When a secondary attracting body orbiting the primary is considered in the dynamics of a spacecraft, the motion is usually described in a synodic reference frame which rotates with the primaries, obtaining the well-known ER3BP or CR3BP equations, depending on how the secondary orbit is approximated [15]. Relative motion equations between two spacecraft both subject to the gravitational field of two primaries, can be obtained by differentiating the respective ER3BP or CR3BP equations. However, it is more useful for relative guidance and navigation systems design to adopt a reference frame local to the target, since it eases the integration of measurements acquired by relative positioning sensors, and allows to better understand and to characterize the chaser trajectories as seen from the target.

Figure 1 shows the Moon-centered synodic reference frame and the target-centered LVLH frame. The rotating coordinate system is defined as $\mathcal{M}_{syn} = \{M; \boldsymbol{i_m}, \boldsymbol{j_m}, \boldsymbol{k_m}\}$, where M denotes the Moon center of mass and the unit vectors are defined as:

- $\boldsymbol{i_m} = -\boldsymbol{r_{em}}/\|\boldsymbol{r_{em}}\|$ where $\boldsymbol{r_{em}}$ is the position vector of the Moon w.r.t. Earth;
- $\boldsymbol{k_m} = \boldsymbol{h_{em}}/\|\boldsymbol{h_{em}}\|$ where $\boldsymbol{h_{em}}$ is the Moon angular momentum vector;
- $\boldsymbol{j_m} = \boldsymbol{k_m} \times \boldsymbol{i_m}$ completes the right-handed coordinate system.

The LVLH frame is $\mathcal{L} = \{\boldsymbol{r_{mt}}; \boldsymbol{i_l}, \boldsymbol{j_l}, \boldsymbol{k_l}\}$, where $\boldsymbol{r_{mt}}$ is the position vector of the target w.r.t. the Moon, and the unit vectors are:

- $\boldsymbol{k_l} = -\boldsymbol{r_{mt}}/\|\boldsymbol{r_{mt}}\|$;
- $\boldsymbol{j_l} = -\boldsymbol{h_{mt}}/\|\boldsymbol{h_{mt}}\|$, where $\boldsymbol{h_{mt}} = \boldsymbol{r_{mt}} \times \dot{\boldsymbol{r}}_{\boldsymbol{mt}}$ is the target angular momentum w.r.t. $\mathcal{M}_{syn}$;
- $\boldsymbol{i_l} = \boldsymbol{j_l} \times \boldsymbol{k_l}$ completes the right-handed coordinate system.

The unit vectors $\boldsymbol{i_l}$, $\boldsymbol{j_l}$ and $\boldsymbol{k_l}$ in the rendezvous literature are generally referred to (with a little abuse of notation) as V-bar (or $\bar{\boldsymbol{V}}$), H-bar (or $\bar{\boldsymbol{H}}$), and R-bar (or $\bar{\boldsymbol{R}}$), respectively [3]. In the classical Keplerian case, $\bar{\boldsymbol{R}}$ and $\bar{\boldsymbol{V}}$ axes define the target orbital plane with respect to the primary, with $\bar{\boldsymbol{H}}$ being always orthogonal to it. Therefore, the *in-track* position of the chaser is defined in the $\bar{\boldsymbol{R}}$-$\bar{\boldsymbol{V}}$ plane, whereas the $\bar{\boldsymbol{R}}$-$\bar{\boldsymbol{H}}$ plane defines the *cross-track* position. However, the target NRHO is a highly non-Keplerian orbit, which does not lie on a plane, therefore the definition adopted in this Note is not strictly equivalent to the one used, for instance, in [3] and [13]. The figure also depicts the chaser position vector w.r.t. the Moon $\boldsymbol{r_{mc}}$ and the position vector relative to the target $\boldsymbol{\rho} = \boldsymbol{r_{mc}} - \boldsymbol{r_{mt}}$.

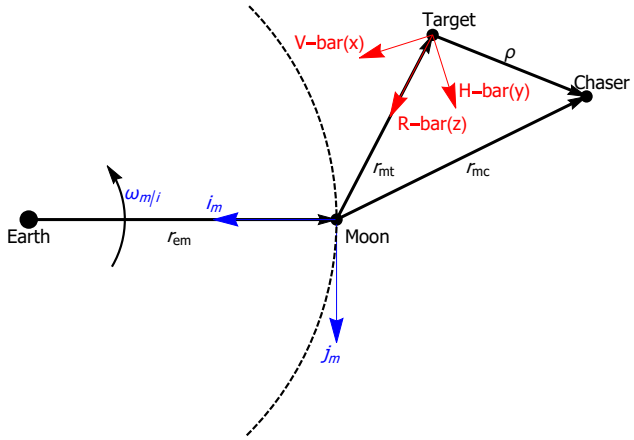

Fig. 1 Definition of vectors and coordinate systems for relative motion.

The equations of relative motion in the LVLH frame and in nondimensional units are given in Eq. (1). The complete derivation can be found in [14].

$$\begin{aligned}\ddot{\boldsymbol{\rho}}\big|_{\mathcal{L}} = &-\mu\frac{\boldsymbol{r_{mt}}+\boldsymbol{\rho}}{\|\boldsymbol{r_{mt}}+\boldsymbol{\rho}\|^3}-(1-\mu)\left(\frac{\boldsymbol{r_{mt}}+\boldsymbol{\rho}+\boldsymbol{r_{em}}}{\|\boldsymbol{r_{mt}}+\boldsymbol{\rho}+\boldsymbol{r_{em}}\|^3}\right)\\ &+\mu\frac{\boldsymbol{r_{mt}}}{\|\boldsymbol{r_{mt}}\|^3}+(1-\mu)\left(\frac{\boldsymbol{r_{mt}}+\boldsymbol{r_{em}}}{\|\boldsymbol{r_{mt}}+\boldsymbol{r_{em}}\|^3}\right)\\ &-2\boldsymbol{\omega_{I/i}}\times\dot{\boldsymbol{\rho}}\big|_{\mathcal{L}}-\dot{\boldsymbol{\omega}}_{\boldsymbol{I/i}}\big|_{\mathcal{L}}\times\boldsymbol{\rho}-\boldsymbol{\omega_{I/i}}\times(\boldsymbol{\omega_{I/i}}\times\boldsymbol{\rho})\end{aligned} \tag{1}$$

where μ is the Earth-Moon mass parameter, $\dot{\boldsymbol{\rho}}\big|_{\mathcal{L}}$ and $\ddot{\boldsymbol{\rho}}\big|_{\mathcal{L}}$ are the relative velocity and acceleration as seen in the LVLH frame, whereas $\boldsymbol{\omega_{I/i}}$ and $\dot{\boldsymbol{\omega}}_{\boldsymbol{I/i}}\big|_{\mathcal{L}}$ are the angular velocity and angular acceleration of the LVLH frame w.r.t. an inertial reference frame $\mathcal{I}$.

No assumptions have been made so far about the Moon motion. However, the above nonlinear and time-varying equations of relative motion can be simplified if a Keplerian orbit is considered for the Moon. This way, the quantities depending on Moon orbital motion can be computed with the classical two-body problem equations. In particular, if an elliptic motion is assumed for the Moon, the obtained equations are referred to as the Elliptic Nonlinear Equations of Relative Motion (ENERM), otherwise, we have the so-called Circular Nonlinear Equations of Relative Motion (CNERM).

By linearizing around target position, we obtain the Elliptic Linear Equations of Relative Motion (ELERM), or the Circular Linear Equations of Relative Motion (CLERM), depending on how the Moon orbit is approximated. The resulting equations have the form $\dot{\boldsymbol{x}}(t)=\boldsymbol{A}(t)\boldsymbol{x}(t)+\boldsymbol{B}\boldsymbol{u}(t)$, where $\boldsymbol{x}=\begin{bmatrix}x & y & z & \dot{x} & \dot{y} & \dot{z}\end{bmatrix}$ is the relative state comprising the relative position and velocity vectors components in the LVLH frame, whereas $\boldsymbol{u}(t)$ is the chaser acceleration vector. The state and the input matrices $\boldsymbol{A}(t)$ and $\boldsymbol{B}(t)$ of these sets of linear and time-varying equations, as well as the solution of the equations in terms of the State Transition Matrix (STM) for impulsive maneuvers, are reported in the Appendix for the reader's clarity.

III. Rendezvous Scenario

The reference mission scenario is based on the HERACLES study [1]. A small lander with a rover and an ascent module will land near the lunar South Pole and will be monitered from the lunar Gateway. The ascent module carrying the sample container will rendezvous and berth with the Gateway, and lunar samples will be transferred to Earth through NASA/Orion capsule. At steady state, this procedure shall operate in the presence and/or absence of astronauts in the Gateway. In this work, the target orbit is a southern NRHO of the Earth-Moon L2 Lagrange point, with maximum distance from the Moon of about 70 thousand kilometers and an average period of about $T = 6.3$ days. This type of orbit exists exactly in the Circular Restricted Three-Body Problem. However, gravitational forces from other celestial bodies (mostly the Sun), and perturbing forces such as the Solar Radiation Pressure, make this orbit unstable and only quasi-periodic. Generally, the initial conditions in terms of position and velocity that generate a quasi-periodic NRHO in a high-fidelity Ephemeris model are obtained by numerically adjusting "patch points" from a NRHO of the CR3BP [16].

The reference orbit, provided by ESA, is shown in Fig. 2 in the Moon-centered rotating frame $\mathcal{M}_{syn}$, corresponding to an initial Epoch time of 00:21 Jan. 09 2020 (Greenwich Mean Time) and propagated for one month.

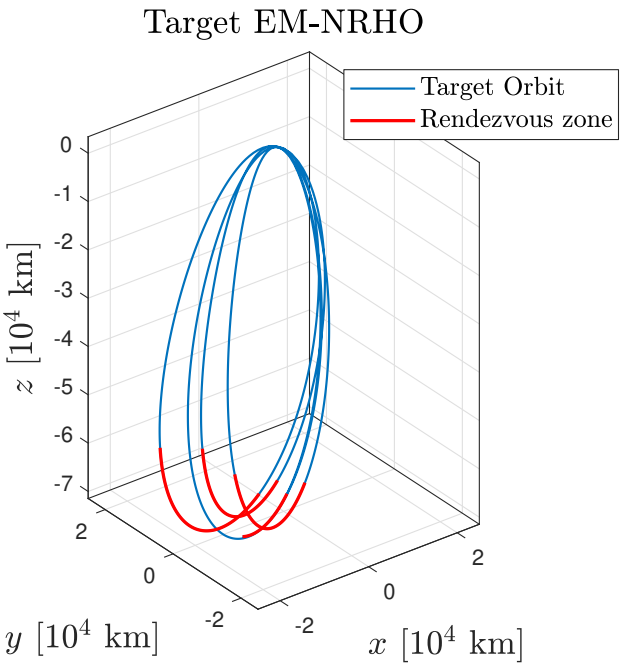

Fig. 2 Target Near Rectilinear Halo Orbit in Moon-centered rotating frame.

By defining the mean anomaly as $M(t) = 2\pi\frac{t}{T}$, where t is the time from the periselene passage, the safer regions for the close-range rendezvous phase (red coloured in Fig. 2), are in the range $M \in [80°, 280°]$ [17], [14], and represents the rendezvous at the aposelene.

The rendezvous is assumed here to start at a relative range of about 50 km, since bearings-only camera sensors have been proven to be usable at these distances. The arrival position is assumed 1 km away from the target, where additional

navigation sensors may be used and tight closed-loop guidance algorithms are needed to ensure more accuracy and operation safety for performing the final approach to the target station.

At these relative distances, and in the aposelene region, the linearized equations can predict relative position and velocity with sufficiently small error with respect to the nonlinear equations [14]. Therefore, both ELERM and CLERM are considered suitable for the analysis and the design of relative guidance, navigation and control systems in the defined scenario.

IV. Bearings-Only Guidance and Navigation

This section describes the guidance and navigation algorithms, using the relative motion presented in Sec. II, as applied to the scenario summarized in Sec. III.

The concept of angles-only or bearings-only navigation is quite basic: by measuring line-of-sight angles (azimuth and elevation) from a reference location to another object of interest, relative position and velocity are determined. Then, if position and velocity of one point are known, position and velocity of the other object might be derived.

A. Bearings-Only Observability

Since the chaser spacecraft is able to measure relative angles only to the target, the relative distance must be estimated by the navigation system. The azimuth θ and elevation ϕ angles as well as the angles-only measurement equations are defined in the Appendix.

Assuming to have a measurement consisting of two angles θ and ϕ, with the relative state vector $\boldsymbol{x} = \left[\rho^T \ \dot{\rho}|_{\mathcal{L}}^T \right]^T \in R^6$, at least three measurements are needed to estimate the whole initial relative state $\boldsymbol{x_0}$. Writing the measurement equations corresponding to three consecutive measurement instants, and exploiting the state solution of the linearized dynamics, it can be concluded that maneuvers must be executed to render observability, and in particular the maneuver performed at time t_0 must produce a measurement at time t_1 different from the measurement that would be obtained without it.

The proof is similar to the one given, for instance, in [7], with the difference being in the relative motion model adopted. Indeed, the authors used the linear and time-invariant HCW equations, for which an analytic solution exists. Here, the linearized relative dynamics include time-varying parameters related to both Moon and target quantities, if the ELERM are considered, and to target quantities only, if the CLERM are used instead. Moreover, since ELERM and CLERM are based on the ER3BP and on the CR3BP, respectively, they cannot be solved analytically.

Let $\boldsymbol{\Phi}(t_1, t_0)$ be the STM between time instants t_0 and t_1 of the linearized relative dynamic equations, and let $\boldsymbol{G}(t_1, t_0)$ the input matrix solution corresponding to an impulsive maneuver performed at initial time t_0 (see the Appendix for details). The necessary condition for observability is then given by Eq. (2) :

$$\boldsymbol{\Phi_p}(t_1, t_0)\boldsymbol{x_0} \neq \boldsymbol{\Phi_p}(t_1, t_0)\boldsymbol{x_0} + \boldsymbol{G_p}(t_1, t_0)\boldsymbol{u} \tag{2}$$

where $\boldsymbol{\Phi_p}(t_1, t_0)$ and $\boldsymbol{G_p}(t_1, t_0)$ are the blocks of $\boldsymbol{\Phi}(t_1, t_0)$ and $\boldsymbol{G}(t_1, t_0)$ corresponding to the position part of the relative state vector, and $\boldsymbol{u}$ is the chaser impulsive acceleration at initial time t_0. This condition can also be used to define an observability cost associated to the maneuver. Indeed, in order to maximize the difference between the free trajectory and the controlled one, the scalar product between the two terms in Eq. (2) must be minimized, obtaining the following objective function:

$$J_{obs}(\boldsymbol{u}, \mathbf{x}_0, t_0, t_1) = (\boldsymbol{\Phi_p}(t_1, t_0)\boldsymbol{x_0})^T (\boldsymbol{\Phi_p}(t_1, t_0)\boldsymbol{x_0} + \boldsymbol{G_p}(t_1, t_0)\boldsymbol{u}) \tag{3}$$

By minimizing $J_{obs}(\boldsymbol{u}, \mathbf{x}_0, t_0, t_1)$, the maneuver $\boldsymbol{u}$ performed at time t_0 with initial relative state $\boldsymbol{x_0}$ can be computed, which maximizes the observability at time t_1. The instant t_1 could be the next instant in which an estimate from the navigation system is acquired, thus reducing the error on the relative range estimate by improving observability through the performed maneuver.

Figures 3 and 4 show the observability trend and the relative range over 5 hours with a chaser position of 20 km behind the target on the V-bar axis, with no initial relative velocity. For 100 uniformly distributed impulsive maneuver directions at time t_0, with magnitude $\|\boldsymbol{u}\| = 1\ m/s$, the observability objective of Eq. (3) is computed. The resulting relative range throughout the 100 trajectories is evaluated as well. Three optimal cases at three different instants are plotted (see t_1 in Eq. (3), for $t_1 = 0.75\ h$, $t_2 = 1.75\ h$ and $t_3 = 4.5\ h$, respectively). With the specified initial conditions, the resulting observability trend is such that the maneuver, which optimizes observability at time t_1, is the same for t_2 and t_3. Consequently, the same maneuver maximizes observability throughout the whole trajectory, which also ensures minimum range in all instants, as in Fig. 4. This is not the case when initial conditions include non-zero relative velocity, as depicted in Figures 5 and 6, where an initial relative velocity of $-2m/s$ on the R-bar axis is assumed. It can be seen how the desired instant in which the maximum observability is required affects the maneuver direction, and therefore the corresponding trajectory as well. The three optimal cases produce three different trajectories. Moreover, Figures 4 and 6 show that the optimal maneuver for observability at a certain instant also yields the minimum value of range at that instant, if compared to all other trajectories. This is reasonable: if range decreases, range observability improves.

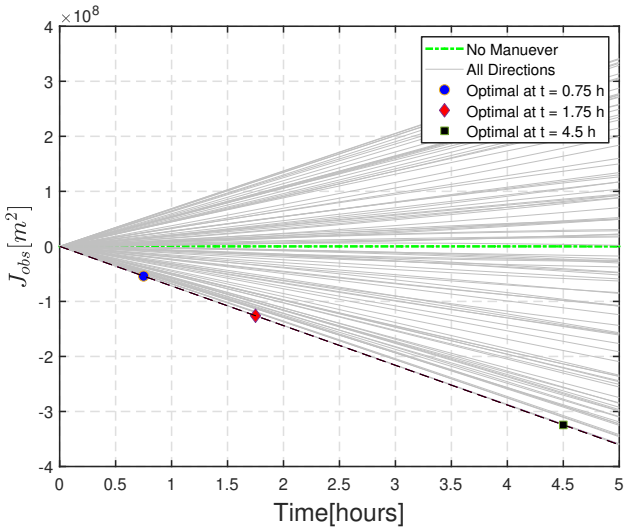

Fig. 3 Observability objective with zero initial relative velocity.

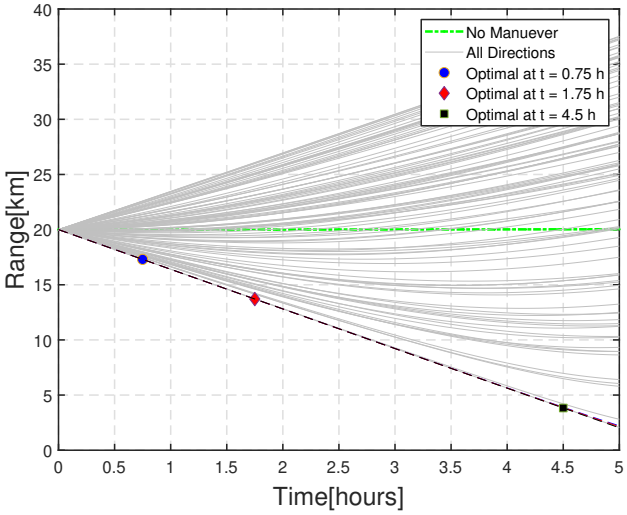

Fig. 4 Range with zero initial relative velocity.

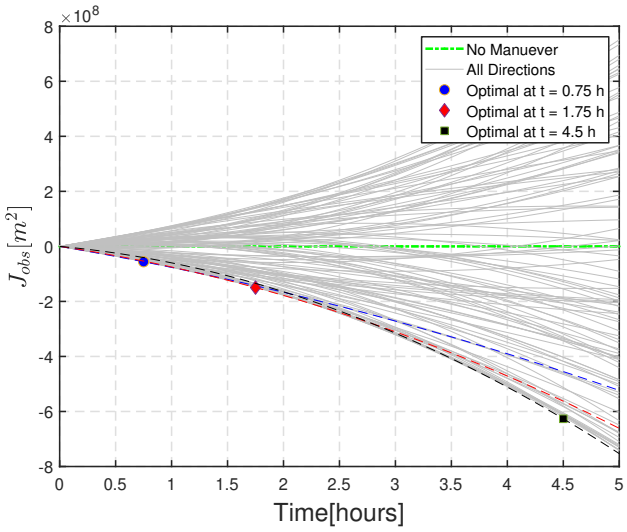

Fig. 5 Observability objective trend with non-zero initial relative velocity.

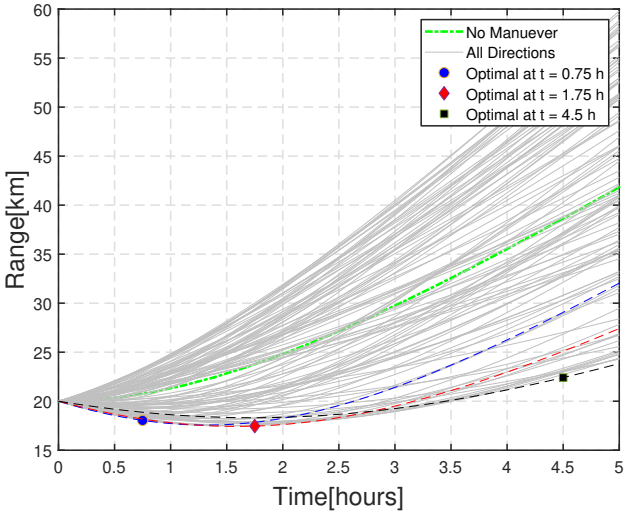

Fig. 6 Range with non-zero initial relative velocity.

B. Fuel-Observability Optimal Guidance

An online multi-impulse and open-loop optimal guidance algorithm is exploited for the defined rendezvous scenario, with a linear-quadratic objective function consisting of a trade-off between fuel consumption and observability, as proposed in [13], and a relative motion model based on the restricted three-body problem assumption. The rendezvous duration t_f and the final desired relative state $\boldsymbol{x}_f$ are fixed. Every T_r seconds, the guidance profile is updated, based on the current relative state estimate, and the trajectory is subdivided into n intervals of duration $\Delta t = \frac{t_{left}}{n}$, where t_{left} is the remaining time to t_f.

The optimization decision vector $\boldsymbol{\alpha} = \left[\boldsymbol{X}_{\in \mathbb{R}^{6(n+1)}} \; \boldsymbol{U}_{\in \mathbb{R}^{3(n+1)}} \; \boldsymbol{S}_{\in \mathbb{R}^{3(n+1)}} \right] \in \mathbb{R}^{12(n+1)}$ includes the $n+1$ relative state

vectors in all discretization time instants $\boldsymbol{X} = \left[\boldsymbol{x}(t_0)\ \boldsymbol{x}(t_1)\ ...\ \boldsymbol{x}(t_n)\right]$, the corresponding impulsive maneuvers $\boldsymbol{U} = \left[\boldsymbol{u}(t_0)\ \boldsymbol{u}(t_1)\ ...\ \boldsymbol{u}(t_n)\right]$, and the auxiliary variables $\boldsymbol{S} = \left[\boldsymbol{s}(t_0)\ \boldsymbol{s}(t_1)\ ...\ \boldsymbol{s}(t_n)\right]$.

The optimal guidance problem is set up as follows:

$$\begin{aligned} \underset{\boldsymbol{\alpha}}{\text{minimize}} \quad & J = wJ_{obs} + (1-w)J_{fuel} \\ \text{subject to} \quad & \boldsymbol{A}_{EOM}\boldsymbol{\alpha} = \boldsymbol{b}_{EOM} \\ & \boldsymbol{A}_{BC}\boldsymbol{\alpha} = \boldsymbol{b}_{BC} \\ & \boldsymbol{A}_{u}\boldsymbol{\alpha} \leq \boldsymbol{b}_{u} \\ & \boldsymbol{A}_{f}\boldsymbol{\alpha} \leq \boldsymbol{b}_{f} \end{aligned} \tag{4}$$

The parameter w is the observability weight. As it will be shown, this parameter has a large impact on the final performance. The fuel-observability cost J and the four constraints in Eq.(4) are defined as in [13] with the only exception being in the computation of the STMs of the relative motion equations. Indeed, let $\boldsymbol{\Phi}(t_{i+1}, t_i)$ be the STM corresponding to either the ELERM or the CLERM, there is a dependence on both initial and final time instants t_i and t_{i+1}, because of the time-varying nature of the equations of relative motion with the third-body perturbation. This affects the expressions (reported in the Appendix) of the observability cost J_{obs} and of the matrix $\boldsymbol{A}_{EOM}$ in the first constraint, which forces the relative states to satisfy the linearized equations of relative motion at each time step. The second constraint imposes the boundary conditions $\boldsymbol{b}_{BC} = [\hat{\boldsymbol{x}}_{\boldsymbol{k}}^T\ \boldsymbol{x}_{\boldsymbol{f}}^T]^T$, where $\hat{\boldsymbol{x}}_{\boldsymbol{k}}$ is the relative state estimate provided by the angles-only navigation filter at the re-planning instant. The third constraint of the optimization problem takes into account the physical limits of the propulsion system, which limits the achievable magnitude of the impulsive maneuvers. The last constraint involves the auxiliary variables that are needed to express the fuel cost (which is the total ΔV consumption) as a linear function of the maneuvers.

The overall objective function is then composed of a linear part J_{fuel}, related to fuel consumption, and of a quadratic part J_{obs} associated to observability. Therefore, the resulting optimization problem can be solved trough a Linear-Quadratic Programming (LQP) routine. Every T_r seconds, starting from the initial conditions given by the navigation filter, the optimization problem is reinitialized, solved, and the maneuvers computed are performed until the next re-planning, as a Model Predictive Control with receding horizon. A diagram of the guidance algorithm is shown in Fig. 7.

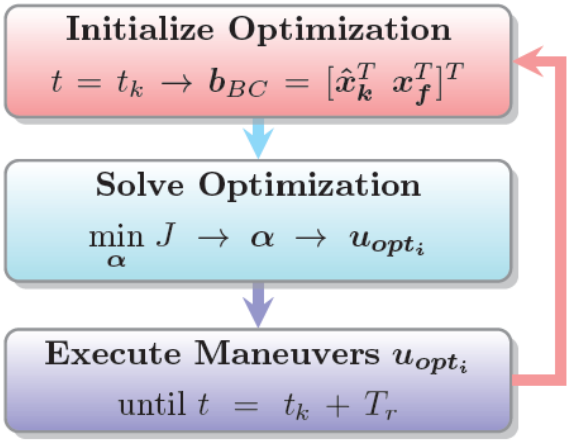

Fig. 7 Guidance algorithm.

In order to reduce the computation time required by the guidance system to compute the chaser maneuvers at each re-planning instant, the STMs necessary by the optimization algorithm are computed as in Eq. (5):

$$\boldsymbol{\Phi}(t + \Delta t, t) \approx exp(\boldsymbol{A}(t) * \Delta t) \tag{5}$$

where the error resulting from the approximation depends on the discretization time step Δt, and on how fast the parameters in $\boldsymbol{A}(t)$ vary. Indeed, simulations have shown that the time-varying parameters of the equations of relative motion with third-body perturbation are much slower in the rendezvous zone of the target Near Rectilinear Halo Orbit, that is near the aposelene. Therefore, the STMs of either the ELERM or the CLERM are computed without solving the differential equations, since only the state matrices $\boldsymbol{A}(t)$ at each discretization instant are needed. These matrices depend on Moon and target quantities only, the former being computed with either the ER3BP of the CR3BP equations, and the latter with the two-body problem equations. In order to verify the validity of the approximation, the ELERM are integrated forward in time for different durations, precisely for $t_f = 45\ min$ to $t_f = 6\ h$, and for different values of the target initial mean anomaly $M(0) \in [0°, 360°]$. Then, every trajectory is compared to the one obtained by propagating the initial state, always fixed to $\boldsymbol{x_0} = \left[-50km\ 0\ 0\ 0\ 0\ 0 \right]^T$, through the State Transition Matrix computed by the approximation of Eq. (5). The index used to assess the accuracy is the aggregate performance index defined as in [18] and reported below:

$$\nu = \max_{0 \le t \le t_f} \left\| \begin{bmatrix} \boldsymbol{\rho} \\ n\dot{\boldsymbol{\rho}} \end{bmatrix} - \begin{bmatrix} \hat{\boldsymbol{\rho}} \\ n\hat{\dot{\boldsymbol{\rho}}} \end{bmatrix} \right\|$$

where the quantities without hat are the relative position and velocity computed integrating the ELERM, whereas the values with hat are computed by means of the approximation, and n is the target NRHO mean motion. This index uses

the target mean motion to normalize time in relative velocity, yielding a metric in distance units suitable to characterize the overall accuracy. In particular, higher values of this parameter indicate higher error. Figure 8 shows the values of ν in a logarithmic scale, with the lower values in the aposelene region confirming that the approximation can be considered valid in this zone. When the rendezvous is performed near the aposelene, this approximation can then be used to ease the maneuvers computation by the guidance algorithm. Note that in the aposelene region it might be possible to simplify the dynamics even further by adopting the CR3BP assumption and therefore the CLERM equations instead of the ELERM.

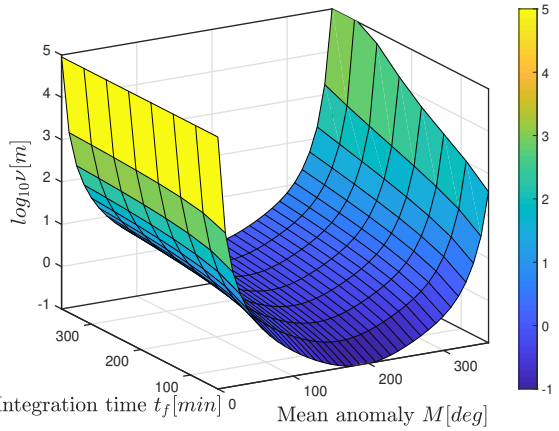

Fig. 8 Errors evaluation of the approximated STM solution of Eq. (5).

The navigation system consists of an Extended Kalman Filter based on the ENERM given in Eq. (1) and on angles-only measurement equations with additive Gaussian noise.

Direct application of the EKF to angles-only navigation could lead to cases of ill-conditioning. This can be alleviated using angles-only measurement equations in spherical coordinates [19]. This way, the measurement equations are linear, leading to better filter performance, and convergence in all cases analyzed in the paper. Some authors have obtained better results with bearings-only navigation by using the Unscented Kalman Filter [20]. However, since the scope of the present work is to analyze the potential of the application of a fuel-observablity guidance scheme for rendezvous in a three-body scenario, the selection of the estimation algorithm is not intended to be optimal, but is made in order to have a complete guidance structure. Future work will validate the proposed guidance with different navigation filters.

A flowchart of the complete guidance and navigation system is shown in Fig. 9.

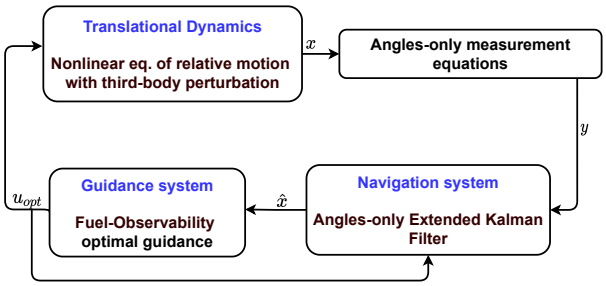

Fig. 9 Complete guidance and navigation architecture.

V. Results

This section presents numerical simulations of the proposed guidance, to the scenario described in Sec. III.

The rendezvous phase is assumed to begin when the target is near the aposelene, which corresponds to an initial target Mean Anomaly of $M(0) = 180°$, in the center of the safe region as previously discussed. This also allows to simplify the computation of the STM of the linearized equations of relative motion (either the ELERM or CLERM) that must be computed by the guidance system in order to initialize the optimization problem at every replan instant. Results relative to achieving berthing at exactly 180 degrees do not show appreciable differences. The initial chaser position is assumed to be behind the target on the V-bar axis, at a distance of 50 km, the final desired relative position is -1 km on the same axis, and the rendezvous duration is fixed to $t_f = 6$ hours. Initial and final relative velocity are assumed equal to zero. The particular initial state on the V-Bar axis was selected as an example taken from [1], and analysis of more general initial conditions and times of flight is not part of this work.

The ENERM (Eq. (1)) are used to propagate the relative state and dynamics model of the navigation filter, therefore no other perturbations besides third-body effects are considered. Moreover, no maneuvers execution errors are considered in the simulations. Indeed, the focus of this work is to assess the ability of the observability optimal guidance to improve performances of the angles-only navigation filter when applied to three-body problem-based relative dynamics models.

The main parameters of the guidance algorithm are the observability weight w, the time interval between maneuvers replans T_r and the time interval Δt through which the trajectory is discretized for each optimization problem. The guidance algorithm is initialized by setting the initial position and velocity of the target with respect to the Moon. Therefore is assumed that the chaser's onboard computer is provided with precise information of target orbit, whereas its relative state to the target is known with some level of uncertainty.

The navigation filter parameters are the initial state covariance matrix $\boldsymbol{P_0} \in \mathbb{R}^{6\times6}$, the covariance matrices of the Gaussian process noise and of the Gaussian measurement noise, $\boldsymbol{Q} \in \mathbb{R}^{6\times6}$ and $\boldsymbol{R} \in \mathbb{R}^{2\times2}$, respectively, and the initial uncertainty in the relative state between the two spacecraft, given in the LVLH frame. Every T_s seconds, a new measurement is acquired and the filter updates the relative state estimate. The simulation parameters used are summarized in Table 1.

Table 1 Simulation parameters

Parameter	Description	Value
$\boldsymbol{x_0}$	Initial nominal relative state [km , km/s]	$\begin{bmatrix} -50 & 0 & 0 & 0 & 0 & 0 \end{bmatrix}$
$\boldsymbol{x_f}$	Desired final relative state [km , km/s]	$\begin{bmatrix} -1 & 0 & 0 & 0 & 0 & 0 \end{bmatrix}$
$M(0)$	Initial target mean anomaly [deg]	180
T	Target NRHO period [days]	6.3
t_f	Rendezvous duration [h]	6
T_r	Time between maneuvers profile updates [min]	45
Δt	Trajectory discretization step [min]	9
T_s	Filter time step [s]	10
$\boldsymbol{P_0}$	Initial covariance matrix [m^2 , m^2/s^2]	$diag(([100\,100\,100\,0.1\,0.1\,0.1]\,/3)^2)$
$\boldsymbol{R}$	Measurement noise covariance matrix [rad^2]	$diag(([1e^{-3}\,1e^{-3}]\,/3)^2)$
$\boldsymbol{Q}$	Process noise covariance matrix [m^2 , m^2/s^2]	$diag(([0\,0\,0\,100\,100\,100]\,/3T)^2)/T_s$

Figure 10 shows that when neglecting the observability in the guidance algorithm by setting $w = 0$, the final position error increases with the uncertainty in the initial relative state. Indeed, with $w = 0$ a fuel-optimal guidance is exploited for the rendezvous, resulting in a long initial drift period with few maneuvers. If the initial relative position and velocity are known exactly, the final position is quite near to the desired one (shown in the figure as a black square and a red circle, respectively) despite the lack of direct range measurements. But as the uncertainty on the initial relative state vector grows, the navigation error fails to converge quickly enough to guarantee a precise arrival position. This can be seen in the right part of the figure, where the arrival positions for different initial errors are depicted, with position and velocity errors $e_{0,pos}$ and $e_{0,vel}$ on each axis ranging from 0 m to 3 km, and from 0 m to 0.1 m/s, respectively, from the red circle to the orange one. The resulting final error is of the order of a few kilometers.

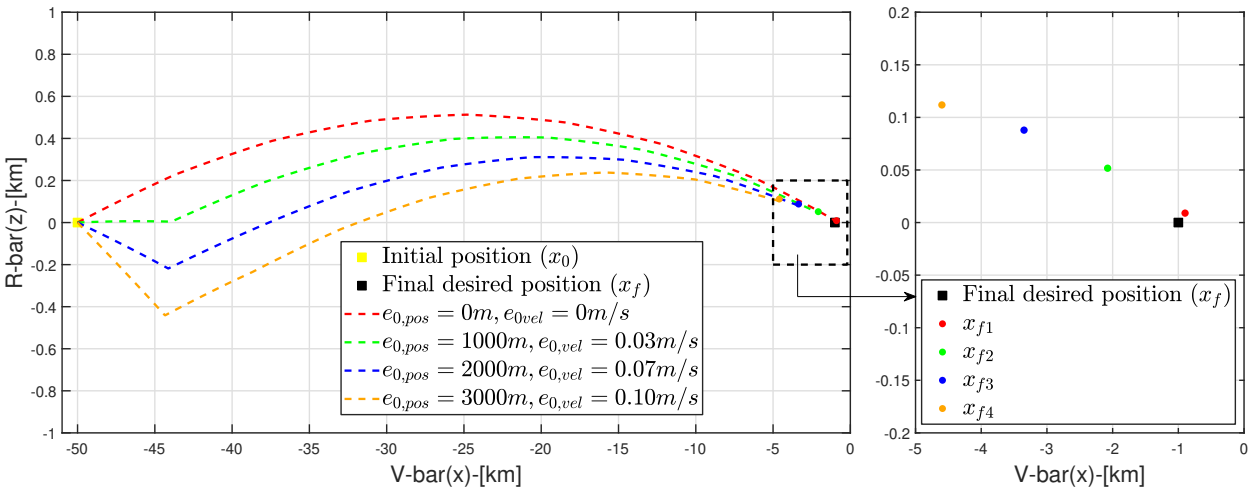

Fig. 10 Rendezvous trajectories for $w = 0$ with increasing uncertainty on the initial relative state.

If observability is taken into account in the guidance algorithm, by setting $w = 0.6$, the final error is much lower, proving that the maneuvers are capable of improving the navigation filter performance, ensuring a faster estimation error convergence even for large initial errors. This is shown in Fig. 11, where the arrival dispersion error is always of the order of a few meters.

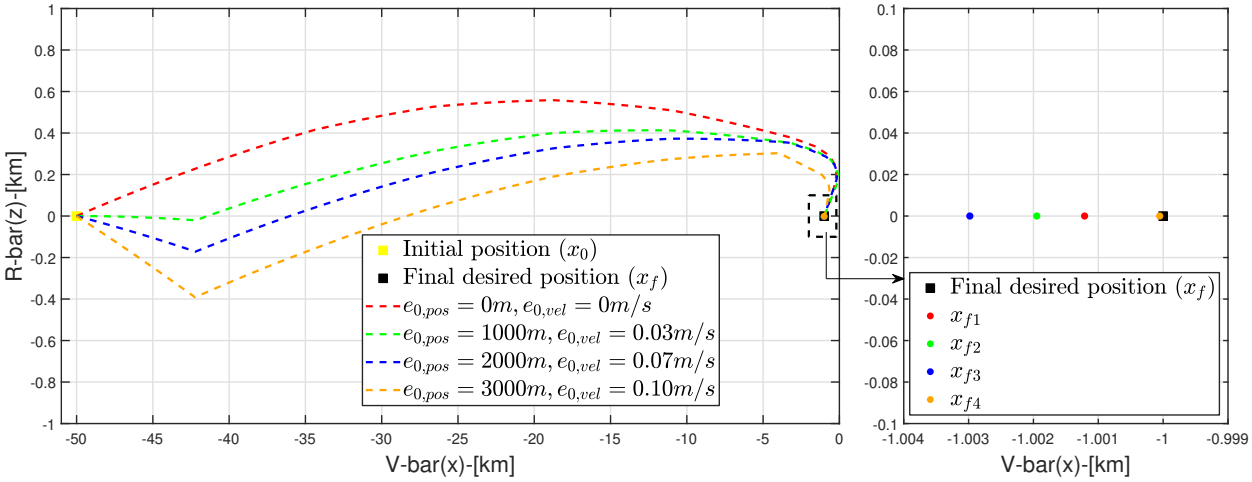

Fig. 11 Rendezvous trajectories for $w = 0.6$ with increasing uncertainty on the initial relative state.

The impact of the observability weight w on navigation system performance can be visualized in Fig. 12, where the range estimation error over time is plotted for different values of w with an initial uncertainty on the relative state equal to the worst case of the previous figures. As w increases from 0 to 0.8, the initial error divergence becomes smaller, allowing for faster convergence and better accuracy in final position, as expected by the expression of the cost function. Indeed, even though the final estimation error is small for $w = 0$, the final position error with respect to the desired one is almost 4 km (the final position corresponds to the orange dot in Fig. 10). This is because when the last maneuvers

profile update is performed (at 45 minutes from the end of the rendezvous), the state estimate is still affected by an error of several hundreds of meters (see the black star on the red line corresponding to the $w = 0$ simulation in Fig. 12).

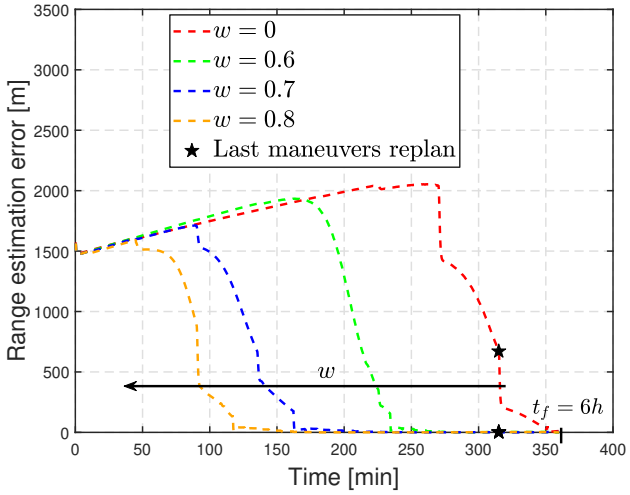

Fig. 12 Range estimation errors vs observability weight.

The downside of including observability in the maneuvers profile computation is a greater fuel consumption in terms of ΔV. However, extensive simulation has shown that with a value of w of about 0.6, an optimal trade-off between navigation performance (and then final position accuracy as well) and total fuel consumption can be achieved. Indeed, for the same reference scenario, the total ΔV with the fuel-optimal guidance is about 6 m/s, and it grows to 7 m/s for $w = 0.6$ and 11 m/s for $w = 0.7$. The final error drops significantly only for values of the observability weight greater than 0.4, and with $w = 0.6$ the position accuracy is of the order of a few meters [21]. Further increase in w does not improve the performance so much, and it makes the total ΔV too large w.r.t. the fuel-optimal case, tripling its value for $w = 0.8$, as depicted in Fig. 13.

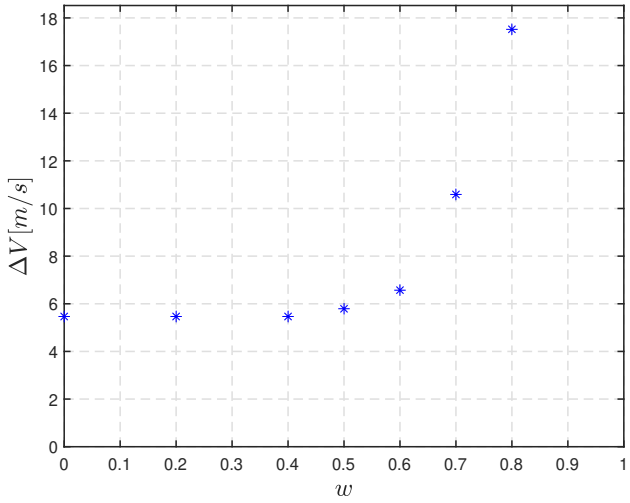

Fig. 13 Fuel consumption vs observability weight.

Finally, the system was tested for different values of the initial relative position, with the V-bar component always equal to $-50\ km$, and H-bar and R-bar ranging from $-20\ km$ to $20\ km$, both with fuel-optimal guidance ($w = 0$) and fuel-observability optimal one with $w = 0.6$. The initial uncertainty in the relative state is set to $3\ km$ and $0.1\ m/s$ on each axis, for every simulation. Figure 14 shows the resulting relative trajectories in the x-z plane of the LVLH frame, as well as the y components over simulation time. The final position obtained in the $w = 0.6$ case (corresponding to the green dashed lines in the plot) is always almost exactly at $\boldsymbol{x}_f$ regardless of the initial conditions, whereas the arrival position when using $w = 0$ appears to be dependent from the starting position. Indeed, as it can be better appreciated in Fig. 15, the final position errors for the $w = 0$ case, depicted as red dots in the figure, range from a few hundred meters to even $3\ km$ or more, as opposed to the very low errors obtained with the observability-enhanced guidance (corresponding to the green squares in the plot).

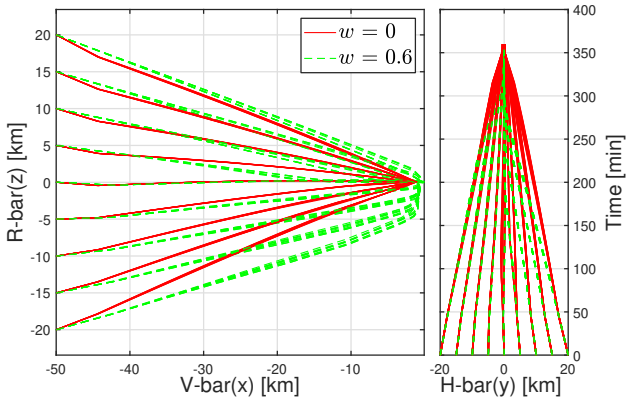

Fig. 14 Trajectories varying initial relative position

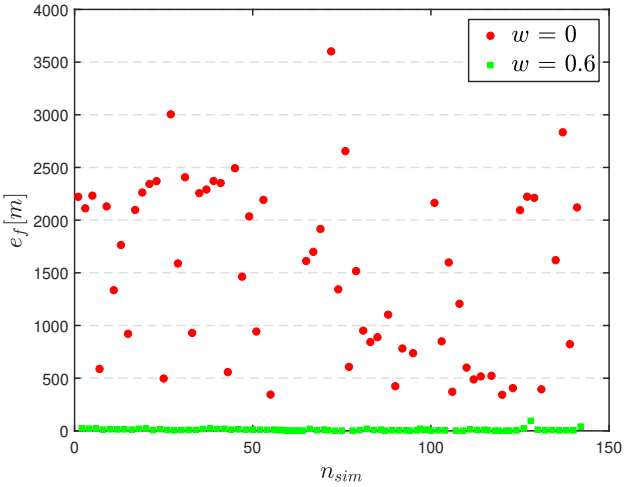

Fig. 15 Final position error

An additional analysis of the guidance performance was carried out in terms of numerical computation, since the CLERM model has fewer time-varying parameters. By repeating the previous test, the results do not change proving

that, in the aposelene region, a relative motion model based on the CR3BP can successfully be employed for guidance system design.

A first comparison example is provided in Fig. 16, which shows the rendezvous trajectories with both ELERM and CLERM cases, obtained with $w = 0.6$ and $M(0) = 165°$, in order to terminate the approach almost exactly at the aposelene. The initial position is $-50\ km$ in the V-Bar direction and the final desired position is again $-1\ km$ on the same axis, with zero relative velocity both at the beginning and at the end of the rendezvous. The final error is about 1.5 meters when the ELERM model is adopted for maneuvers computation, and it is very close to the 1.7 meters error which is obtained with the CLERM.

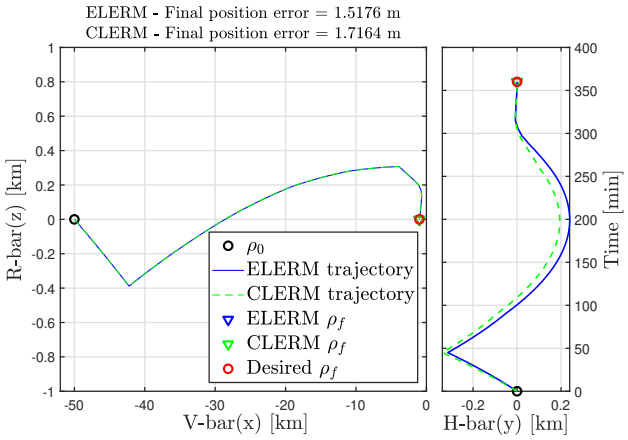

Fig. 16 ELERM - CLERM Trajectory comparison, $\boldsymbol{\rho_0}$ = [-50 , 0 , 0] km, $w = 0.6$

The same comparison is shown in Fig. 17 for different initial conditions. The starting position is set to $\boldsymbol{\rho_0}$ = [-50, 10, 10] km, and the resulting trajectories as well as the final errors obtained with the two models are even more comparable.

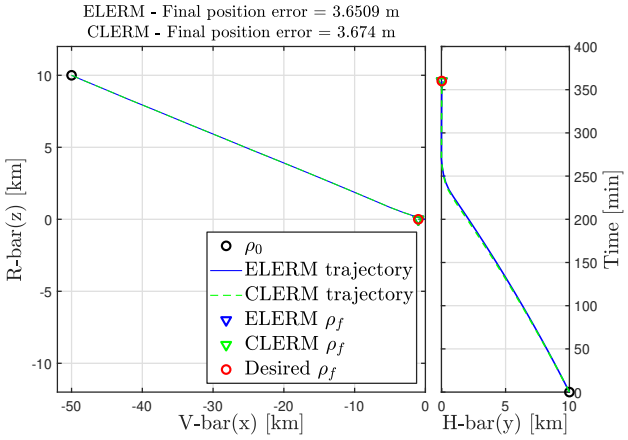

Fig. 17 ELERM - CLERM Trajectory comparison, $\boldsymbol{\rho_0}$ = [-50, 10, 10] km, w = 0.6

The resulting average computational time required by the guidance algorithm to output the maneuvers profile at each re-planning instant, is of the order of 2 seconds when using the ELERM model, and of about one half second less with

the CLERM. Hence, the computation cost of the proposed method could be practical for an onboard implementation, with the CLERM model giving better performances in terms of computation time without adding any significant error with respect to the ELERM.

VI. Conclusions

A fuel-observability optimal guidance with bearings-only navigation is applied to the close-phase of rendezvous in a Near Rectilinear Halo Orbit of the Earth-Moon L2 Lagrange point. Classical relative motion models such as the Hill-Clohessy-Wiltshire or Tschauner-Hempel equations cannot be used in this scenario, because of the highly non-Keplerian orbit of the target. In this work, guidance and navigation algorithms exploit relative translational dynamic with third body perturbation, under the Elliptic Restricted Three-Body Problem assumption, which is considerably more accurate, for rendezvous in a NRHO, than the two-body problem assumption commonly used for GNC design in low Earth orbit. The drawback is the complexity of the model, which does not provide an analytical solution to be used by the guidance system. However, assuming the rendezvous to be performed while the target is near the aposelene of its orbit, the time-varying linearized equations of relative motion can be numerically solved computing the State Transition Matrix in an approximated but sufficiently accurate way. The guidance algorithm computes chaser's maneuvers by solving an optimization problem, which takes into account the complex three-body dynamics and at the same time reduces computation complexity and time by avoiding to numerically solve the differential equations. Moreover, by formulating the rendezvous guidance as a linear-quadratic optimization problem, it should also be straightforward to add additional constraints if needed, such as geometric constraints on the approach trajectory for safety considerations. Possible improvements could be achieved with different navigation filters, because the Extended Kalman Filter, adopted in this Note, can suffer from covariance ill-conditioning when applied to bearings-only navigation.

Appendix A: Definitions

A1. Bearings-Only Measurement Equations

The measurement angles are defined in the target-centered LVLH frame $\mathcal{L}$ defined in Sec. II, as depicted in Fig. A1. The elevation angle ϕ is defined from -90 to 90 deg and the azimuth angle θ spans from 0 to 180 deg.

The resulting angles-only measurement equations are given in Eq. A1:

$$\mathbf{y} = \mathbf{h}(\mathbf{x}) = \begin{bmatrix} \theta \\ \\ \phi \end{bmatrix} = \begin{bmatrix} arctan(y/x) \\ \\ arcsin(z/\sqrt{x^2+y^2+z^2}) \end{bmatrix} \tag{A1}$$

where x, y and z are the components of the relative position vector $\boldsymbol{\rho}$.

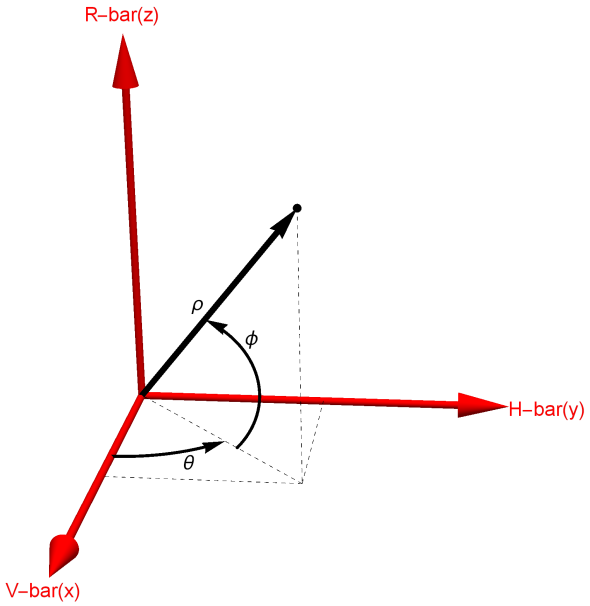

Fig. A1 Chaser elevation (ϕ) and azimuth (θ) angles in LVLH frame

A2. Linearized equations of relative motion

By defining the skew symmetric matrices $\boldsymbol{\Omega_{l/i}}$ and $\dot{\boldsymbol{\Omega}}_{\boldsymbol{l/i}}\big|_{\mathcal{L}}$ associated with the angular velocity $\boldsymbol{\omega_{l/i}}$ and the angular acceleration $\dot{\boldsymbol{\omega}}_{\boldsymbol{l/i}}\big|_{\mathcal{L}}$ of the LVLH frame with respect to inertial frame, respectively, and linearizing around the target position, the nonlinear equations of relative motion given in Eq. (1) become:

$$\begin{aligned}\ddot{\boldsymbol{\rho}}\big|_{\mathcal{L}} = &-2\boldsymbol{\Omega_{l/i}}\ \dot{\boldsymbol{\rho}}\big|_{\mathcal{L}} - (\dot{\boldsymbol{\Omega}}_{\boldsymbol{l/i}}\big|_{\mathcal{L}} + \boldsymbol{\Omega}^2_{\boldsymbol{l/i}})\boldsymbol{\rho} \\ &- \frac{\mu}{\|\boldsymbol{r_{mt}}\|^3}(\boldsymbol{I_{3\times3}} - 3\frac{\boldsymbol{r_{mt}}\boldsymbol{r}_{\boldsymbol{mt}}^T}{\|\boldsymbol{r_{mt}}\|^2})\boldsymbol{\rho} \\ &- \frac{1-\mu}{\|\boldsymbol{r_{mt}}+\boldsymbol{r_{em}}\|^3}(\boldsymbol{I_{3\times3}} - 3\frac{(\boldsymbol{r_{mt}}+\boldsymbol{r_{em}})(\boldsymbol{r_{mt}}+\boldsymbol{r_{em}})^T}{\|\boldsymbol{r_{mt}}+\boldsymbol{r_{em}}\|^2})\boldsymbol{\rho}\end{aligned} \tag{A2}$$

In state-space form, and assuming the chaser controllable in acceleration through the control vector $\boldsymbol{u}(t)$, Eq.(A2) takes the form $\dot{\boldsymbol{x}}(t) = \boldsymbol{A}(t)\boldsymbol{x}(t) + \boldsymbol{B}\boldsymbol{u}(t)$, which is a linear time-varying system, with:

$$
\begin{aligned}
\boldsymbol{x}(t) &= \begin{bmatrix} \boldsymbol{\rho} \\ \dot{\boldsymbol{\rho}}\big|_{\mathcal{L}} \end{bmatrix} \\
\boldsymbol{A}(t) &= \begin{bmatrix} \boldsymbol{O_{3\times3}} & \boldsymbol{I_{3\times3}} \\ \boldsymbol{A_{21}} & -2\boldsymbol{\Omega_{l/i}} \end{bmatrix} \\
\boldsymbol{A_{21}} &= \dot{\boldsymbol{\Omega}}_{\boldsymbol{l/i}}\big|_{\mathcal{L}} + \boldsymbol{\Omega}_{\boldsymbol{l/i}}^2 - \frac{\mu}{\|\boldsymbol{r_{mt}}\|^3}(\boldsymbol{I_{3\times3}} - 3\frac{\boldsymbol{r_{mt}}\boldsymbol{r_{mt}}^T}{\|\boldsymbol{r_{mt}}\|^2}) \\
&\quad - \frac{1-\mu}{\|\boldsymbol{r_{mt}} + \boldsymbol{r_{em}}\|^3}(\boldsymbol{I_{3\times3}} - 3\frac{(\boldsymbol{r_{mt}} + \boldsymbol{r_{em}})(\boldsymbol{r_{mt}} + \boldsymbol{r_{em}})^T}{\|\boldsymbol{r_{mt}} + \boldsymbol{r_{em}}\|^2} \\
\boldsymbol{B} &= \begin{bmatrix} \boldsymbol{O_{3\times3}} \\ \boldsymbol{I_{3\times3}} \end{bmatrix}
\end{aligned}
\tag{A3}
$$

The relative state $\boldsymbol{x}$ at generic instant t_k can be computed as in Eq. A4:

$$
\boldsymbol{x}(t_k) = \boldsymbol{\Phi}(t_k, t_0)\boldsymbol{x}(t_0) + \int_{t_0}^{t_k} \boldsymbol{\Phi}(t, t_0)\boldsymbol{B}\boldsymbol{u}(t)dt \tag{A4}
$$

where $\boldsymbol{\Phi}(t_k, t_0)$ is the STM of the linear and time-varying differential equations given in Eq. (A2).

If an impulsive maneuver $\boldsymbol{u}(t) = \boldsymbol{u}\delta(t - t_0)$ at time t_0 is considered, the solution of the relative motion equations is given by Eq. A5

$$
\boldsymbol{x}(t_k) = \boldsymbol{\Phi}(t_k, t_0)\boldsymbol{x}(t_0) + \boldsymbol{G}(t_k, t_0)\boldsymbol{u} \tag{A5}
$$

where $\boldsymbol{G}(t_k, t_0) = \int_{t_0}^{t_k} \boldsymbol{\Phi}(t, t_0)\boldsymbol{B}\delta(t - t_0)dt = \boldsymbol{\Phi}(t_k, t_0)\boldsymbol{B} \in R^{6\times3}$.

A3. Observability Cost

The observability cost J_{obs} included in the guidance optimization objective of Eq. 4 is defined as:

$$
J_{obs} = \sum_{i=1}^{n} J_{obs_i} \doteq \frac{1}{2}\boldsymbol{\alpha}^T \boldsymbol{A_{obs}}\boldsymbol{\alpha} \tag{A6}
$$

where J_{obs_i} is computed as in Eq. (3), and the symmetric matrix $A_{obs} \in \mathbb{R}^{12(n+1)\times12(n+1)}$ is defined in Eq. A7:

$$\boldsymbol{A_{obs}} = \begin{bmatrix} \boldsymbol{A_x} & \boldsymbol{A_u} & \boldsymbol{O}_{6(n+1)\times 3(n+1)} \\ \boldsymbol{A_u^T} & \boldsymbol{O}_{3(n+1)\times 3(n+1)} & \boldsymbol{O}_{3(n+1)\times 3(n+1)} \\ \boldsymbol{O}_{3(n+1)\times 6(n+1)} & \boldsymbol{O}_{3(n+1)\times 3(n+1)} & \boldsymbol{O}_{3(n+1)\times 3(n+1)} \end{bmatrix}$$

$$\boldsymbol{A_x} = \begin{bmatrix} 2\boldsymbol{\Phi_p}(t_1,t_0)^T\boldsymbol{\Phi_p}(t_1,t_0) & \boldsymbol{O}_{6\times 6} & \dots & \boldsymbol{O}_{6\times 6} \\ \boldsymbol{O}_{6\times 6} & 2\boldsymbol{\Phi_p}(t_2,t_1)^T\boldsymbol{\Phi_p}(t_2,t_1) & \ddots & \vdots \\ \vdots & \ddots & \ddots & \boldsymbol{O}_{6\times 6} \\ \boldsymbol{O}_{6\times 6} & \dots & \boldsymbol{O}_{6\times 6} & 2\boldsymbol{\Phi_p}(t_n,t_{n-1})^T\boldsymbol{\Phi_p}(t_n,t_{n-1}) \end{bmatrix} \tag{A7}$$

$$\boldsymbol{A_u} = \begin{bmatrix} \boldsymbol{\Phi_p}(t_1,t_0)^T\boldsymbol{G_p}(t_1,t_0) & \boldsymbol{O}_{3\times 3} & \dots & \boldsymbol{O}_{3\times 3} \\ \boldsymbol{O}_{3\times 3} & \boldsymbol{\Phi_p}(t_2,t_1)^T\boldsymbol{G_p}(t_2,t_1) & \ddots & \vdots \\ \vdots & \ddots & \ddots & \boldsymbol{O}_{3\times 3} \\ \boldsymbol{O}_{3\times 3} & \dots & \boldsymbol{O}_{3\times 3} & \boldsymbol{\Phi_p}(t_n,t_{n-1})^T\boldsymbol{G_p}(t_n,t_{n-1}) \end{bmatrix}$$

where $\boldsymbol{\Phi_p}(t_{i+1},t_i)$ are the blocks of the STMs corresponding to the position part of the state vector.

A4. Relative Motion Constraints

By employing the ELERM or CLERM solution for impulsive maneuvers in terms of State Transition Matrix as in Eq. (A5), the relative states in the optimization decision vector are forced to satisfy the linearized equations of relative motion with third-body perturbation, under the Elliptic Restricted Three-Body Problem and the Circular Restricted Three-Body Problem assumptions, respectively.

Being $\boldsymbol{x}(t_0)$, $\boldsymbol{x}(t_1)$, $\dots$ $\boldsymbol{x}(t_n)$, the relative states at discretization time instants t_0, t_1 , …, t_n, the following n constraints are imposed:

$$\begin{aligned} t = t_1 &\rightarrow \boldsymbol{x}(t_1) - \boldsymbol{\Phi}(t_1,t_0)\boldsymbol{x}(t_0) - \boldsymbol{G}(t_1,t_0)\boldsymbol{u}(t_0) = 0 \\ t = t_2 &\rightarrow \boldsymbol{x}(t_2) - \boldsymbol{\Phi}(t_2,t_1)\boldsymbol{x}(t_1) - \boldsymbol{G}(t_2,t_1)\boldsymbol{u}(t_1) = 0 \\ &\vdots \\ t = t_n &\rightarrow \boldsymbol{x}(t_n) - \boldsymbol{\Phi}(t_n,t_{n-1})\boldsymbol{x}(t_{n-1}) - \boldsymbol{G}(t_n,t_{n-1})\boldsymbol{u}(t_{n-1}) = 0 \end{aligned} \tag{A8}$$

where $\boldsymbol{G}(t_i, t_{i-1}) = (\boldsymbol{\Phi}(t_i, t_{i-1}) \begin{bmatrix} \boldsymbol{O}_{3\times3} \\ \boldsymbol{I}_{3\times3} \end{bmatrix}) \in \mathbb{R}^{6\times3}$

By collecting in matrix form, we obtain $A_{EOM}\boldsymbol{\alpha} = \boldsymbol{b}_{EOM}$, which are the relative motion constraints of the guidance optimization algorithm (the first constraint in Eq.(4)) with:

$$
\begin{aligned}
\boldsymbol{A_{EOM}} &= \begin{bmatrix} \boldsymbol{A_{EOM_1}} \in \mathbb{R}^{6n\times6(n+1)} & \boldsymbol{A_{EOM_2}} \in \mathbb{R}^{6n\times3(n+1)} & \boldsymbol{O}_{6n\times3(n+1)} \end{bmatrix} \\
\boldsymbol{A_{EOM_1}} &= \begin{bmatrix} -\boldsymbol{\Phi}(t_1,t_0) & \boldsymbol{I}_{3\times3} & \boldsymbol{O}_{3\times3} & \dots & \boldsymbol{O}_{3\times3} \\ \boldsymbol{O}_{3\times3} & -\boldsymbol{\Phi}(t_2,t_1) & \boldsymbol{I}_{3\times3} & \ddots & \vdots \\ \vdots & \ddots & \ddots & \ddots & \boldsymbol{O}_{3\times3} \\ \boldsymbol{O}_{3\times3} & \dots & \boldsymbol{O}_{3\times3} & -\boldsymbol{\Phi}(t_n,t_{n-1}) & \boldsymbol{I}_{3\times3} \end{bmatrix} \\
\boldsymbol{A_{EOM_2}} &= \begin{bmatrix} -\boldsymbol{G}(t_1,t_0) & \boldsymbol{O}_{3\times3} & \dots & \boldsymbol{O}_{3\times3} \\ \boldsymbol{O}_{3\times3} & -\boldsymbol{G}(t_2,t_1) & \ddots & \vdots \\ \vdots & \ddots & \ddots & \boldsymbol{O}_{3\times3} \\ \boldsymbol{O}_{3\times3} & \dots & \boldsymbol{O}_{3\times3} & -\boldsymbol{G}(t_n,t_{n-1}) \end{bmatrix} \\
\boldsymbol{b}_{EOM} &= \boldsymbol{0} \in \mathbb{R}^{6n}
\end{aligned}
\tag{A9}
$$

Acknowledgments

This work was partially supported by the European Space Agency under contract No. 000121575/17/NL/hh. The view expressed herein can in no way be taken to reflect the official opinion of the European Space Agency.

References

[1] Renk, F., Landgraf, M., and Bucci, L., "Refined Mission Analysis for Heracles - a Robotic Lunar Surface Sample Return Mission Utilizing Human Infrastructure," *2018 AAS/AIAA Astrodynamics Specialist Conference*, Paper 18-344, Snowbird, UT, USA, 2018.

[2] Zimovan, E., Howell, K., and Davis, D. C., "Near rectilinear halo orbits and their application in cis-lunar space," *3rd IAA Conference on Dynamics and Controls of Space Systems*, Paper IAA-AAS-DyCoSS3-125, Moscow, Russia, 2017.

[3] Fehse, W., *Automated Rendezvous and Docking of Spacecraft*, Cambridge Aerospace Series, Cambridge University Press, Cambridge, England, U.K., 2003, pp. 31–32. https://doi.org/10.1017/CBO9780511543388.

[4] Gaias, G., and Ardaens, J.-S., "Flight demonstration of autonomous noncooperative rendezvous in low earth orbit," *Journal of Guidance, Control, and Dynamics*, Vol. 41, No. 6, 2017, p. 1337–1354. https://doi.org/10.2514/1.G003239.

[5] Sanchez, H., McIntosh, D., Cannon, H., Pires, C., M-Field, Sullivan, J., D'Amico, S., Mall, L., and O'Connor, B., "Starling-1: swarm technology demonstration," *32nd Annual Small Satellite Conference*, Logan, UT, USA, 2018.

[6] Woffinden, D., and Geller, D., "Observability Criteria for Angles-Only Navigation," *IEEE Transactions on Aerospace and Electronic Systems*, Vol. 45, No. 3, 2009, pp. 1194–1208. https://doi.org/10.1109/TAES.2009.5259193.

[7] Grzymisch, J., and Fichter, W., "Observability Criteria and Unobservable Maneuvers for In-Orbit Bearings-Only Navigation," *Journal of Guidance, Control and Dynamics*, Vol. 37, No. 4, 2014, pp. 1–10. https://doi.org/10.2514/1.62476.

[8] Clohessy, W. H., and Wiltshire, R. S., "Terminal Guidance System for Satellite Rendezvous," *Journal of Guidance, Control, and Dynamics*, Vol. 27, No. 9, 1960, pp. 653–658. https://doi.org/10.2514/8.8704.

[9] Luo, J., Gong, B., Yuan, J., and Zhang, Z., "Angles-only relative navigation and closed-loop guidance or spacecraft proximity operations," *Acta Astronautica*, Vol. 128, 2016, pp. 91–106. https://doi.org/10.1016/j.actaastro.2016.06.032.

[10] Tschauner, J., and Hempel, P., "Rendezvous zu einem in elliptischer Bahn umlaufenden Ziel [Rendezvous with a target in an elliptical orbit]," *Acta Astronautica*, Vol. 11, No. 2, 1965, pp. 104–109.

[11] Woffinden, D., and Geller, D., "Optimal Orbital Rendezvous Maneuvering for Angles-Only Navigation," *Journal of Guidance, Control and Dynamics*, Vol. 32, No. 4, 2009, pp. 1382–1387. https://doi.org/10.2514/1.45006.

[12] Grzymisch, J., and Fichter, W., "Analytic Optimal Observability Maneuvers for In-Orbit Bearings-Only Rendezvous," *Journal of Guidance, Control and Dynamics*, Vol. 37, No. 5, 2014, pp. 1658–1664. https://doi.org/10.2514/1.G000612.

[13] Grzymisch, J., and Fichter, W., "Optimal Rendezvous Guidance with Enhanced Bearings-Only Observability," *Journal of Guidance, Control and Dynamics*, Vol. 38, No. 6, 2015, pp. 1131–1140. https://doi.org/10.2514/1.G000822.

[14] Franzini, G., and Innocenti, M., "Relative Motion Dynamics in the Restricted Three-Body Problem," *Journal of Spacecraft and Rockets*, Vol. 56, No. 5, 2019, pp. 1322–1447. https://doi.org/10.2514/1.A34390.

[15] Koon, W. S., Lo, M. W., E.Marsden, J., and Ross, S. D., *Dynamical Systems, The Three-Body Problem, and Space Mission Design*, Vol. ISBN 978-0-615-24095-4, Marsden Books, 2011.

[16] Qian, Y., Yang, X., Jing, W., and Zhang, W., "An improved numerical method for constructing Halo/Lissajous orbits in a full solar system model," *Chinese Journal of Aeronautics*, Vol. 31, No. 6, 2018, pp. 1362–1374. https://doi.org/10.1016/j.cja.2018.03.006.

[17] Bucci, L., Lavagna, M., and Renk, F., "Relative Dynamics analysis and rendezvous techniques for lunar Near Rectilinear Halo Orbits," *Proc. 68th International Astronautical Congress (IAC 2017)*, Vol. 12, Adelaide, Australia, 2017, pp. 7645–7654.

[18] Sullivan, J., Grimberg, S., and D'Amico, S., "Comprehensive Survey and Assessment of Spacecraft Relative Motion Dynamics Models," *Journal of Guidance, Control and Dynamics*, Vol. 40, No. 8, 2017, pp. 1837–1859. https://doi.org/10.2514/1.G002309.

[19] Mohanty, N. C., "Autonomous Navigation for High Altitude Satellites," *Information Sciences*, Vol. 30, 1983, pp. 125–150. https://doi.org/10.1016/0020-0255(83)90003-8.

[20] Sullivan, J., and D'Amico, S., "Nonlinear Kalman filtering for improved angles-only navigation using relative orbital elements," *Journal of Guidance, Control, and Dynamics*, Vol. 40, No. 9, 2017, p. 2183–2200. https://doi.org/10.2514/1.G002719.

[21] D'Onofrio, F., Bucchioni, G., and Innocenti, M., "Bearings-Only Guidance for Rendezvous in a Cis-Lunar NRHO," *31st AAS/AIAA Space Flight Mechanics Meeting*, Paper 21-209, Charlotte, NC, USA, 2021.